Net heat-flux measurement method for passive radiative cooling materials with ambient self-tracking – SUPPLEMENTARY MATERIAL

Fabio Bertiglia[a], Davide Forte[b], Giuseppina Lopardo[a], Ferruccio Girard[a], Matteo Fasano[b], Lorenzo Pattelli[a]

[a] *Istituto Nazionale di Ricerca Metrologica, Strada delle Cacce 91, Torino, 10135, Italy*
[b] *Department of Energy, Politecnico di Torino, Corso Duca degli Abruzzi 24, Torino, 10129, Italy*

S1. Full experimental campaign data

The RAFT setup was extensively evaluated over a one-month period, from 05/09/2025 to 05/10/2025. Throughout this campaign, all sensors operated continuously, except for a brief power outage on 22–23/09/2025. Figure S1 presents the experimental data collected during the month-long measurement period.

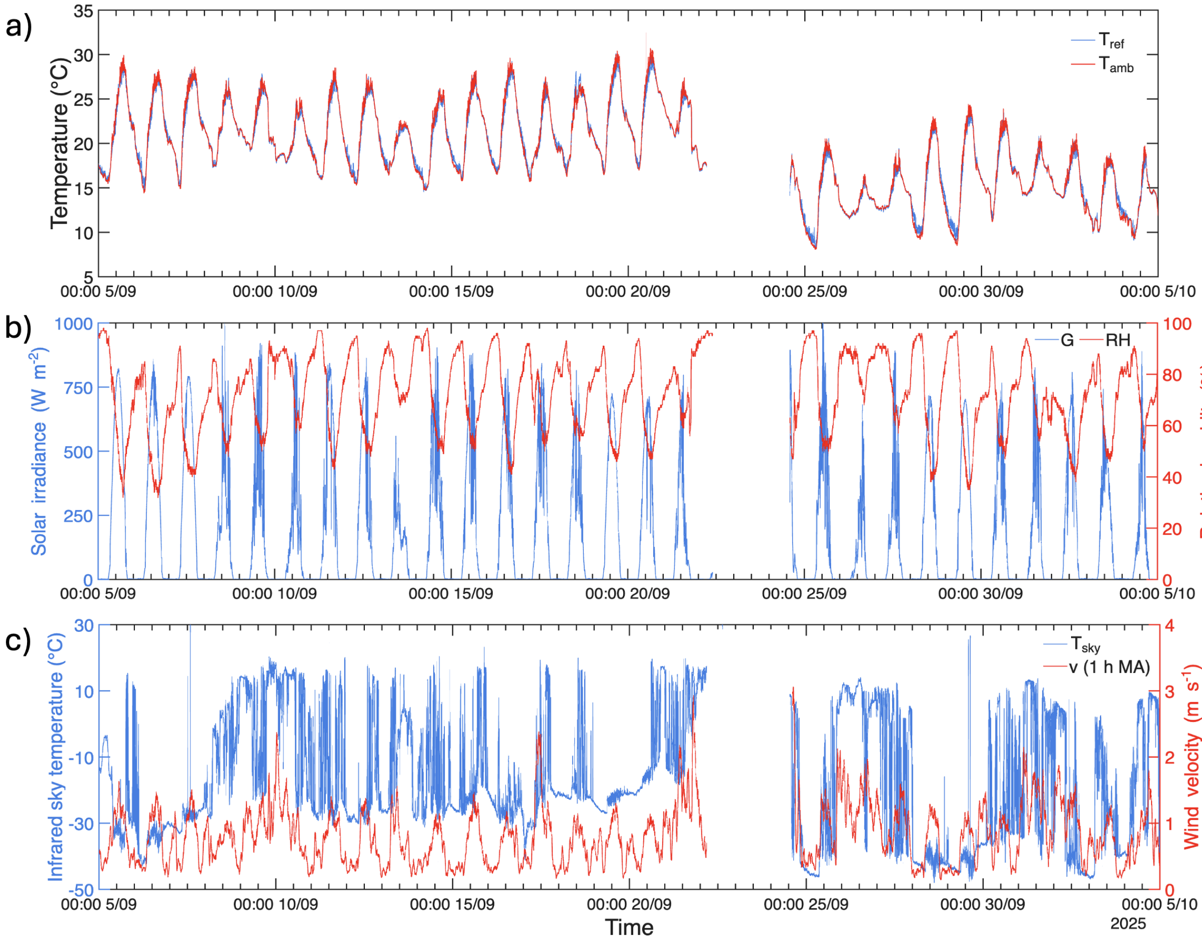

Figure S1: Experimental data acquired from 05/09/2025 to 05/10/2025: a) convective heat exchanger assembly and ambient temperatures; b) solar irradiance and relative humidity; and c) infrared sky temperature and wind velocity.

During the experimental campaign, the RAFT system was exposed to a broad range of atmospheric conditions, including significant variations in relative humidity and wind speed, as well as both clear-sky and overcast conditions. Fig. S2 presents violin plots of the principal atmospheric variables–namely air temperature, relative humidity, wind speed, and infrared sky temperature–together with the temperature of the convective heat exchanger assembly over the entire duration of the experimental campaign. The distributions and average values of T_{ref} and T_{amb} are closely comparable as expected, while T_{sky} shows a broad range of atmospheric irradiance conditions, ranging from apparent temperatures ranging approximately between −50 °C to 20 °C.

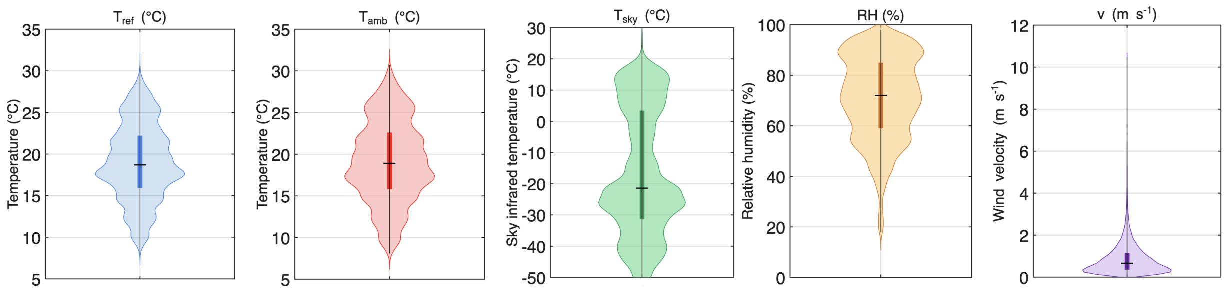

Figure S2: Violin plots of experimental data from RAFT setup 5/09-5/10/2025: convective heat exchanger assembly temperature, air temperature, infrared sky temperature, relative humidity and wind speed

S2. Downwelling longwave atmospheric irradiance

As reported in the main text, the atmospheric flux absorbed by the sample, q_{atm}, is computed using the definition of atmospheric spectral emissivity $\varepsilon_{\mathrm{atm}}(\lambda, \mathrm{RH}, T_{\mathrm{amb}})$. This quantity is evaluated through a polynomial expression, according to the model proposed by Das et al. [1]:

$$\varepsilon_{\mathrm{atm}} = 1 - \exp\left[a_0(\lambda) + a_1(\lambda)w + a_2(\lambda)w^2 + a_3(\lambda)w^3\right] \tag{S1}$$

where w is the precipitable water vapor amount (in cm) and a_0, a_1, a_2, and a_3 are wavelength-dependent functions defined over the spectral range 5.25–42.83 µm. The precipitable water vapor is estimated using the correlation from Ref. [2]:

$$w = 46.5\frac{p_{\mathrm{v}}(T_{\mathrm{amb}})}{T_{\mathrm{amb}}} \tag{S2}$$

with $p_{\mathrm{v}}(T_{\mathrm{amb}})$ the vapor pressure at ambient temperature (in hPa). The vapor pressure is obtained from the relative humidity RH according to the following correlation [3]:

$$p_{\mathrm{v}} = \mathrm{RH}\left[6.1078\exp\left(\frac{17.27(T - 273.15)}{T - 35.85}\right)\right] \tag{S3}$$

The downwelling longwave atmospheric irradiance in clear sky conditions E_{atm} can be modeled as:

$$E_{\mathrm{atm}} = \pi\int_0^\infty \varepsilon_{\mathrm{atm}}(\lambda) I_{\mathrm{b}}(\lambda, T_{\mathrm{amb}})\,\mathrm{d}\lambda \tag{S4}$$

where $I_{\mathrm{b}}(\lambda, T_{\mathrm{amb}})$ is the blackbody spectral radiance at temperature T_{amb}.

The modeled value of E_{atm}, calculated from the meteorological data (RH and T_{amb}) measured during the experimental campaign (6–7 September 2025), was compared with the average downwelling atmospheric radiation from the ERA5 reanalysis database [4]. As shown in Fig. S3a, the two signals are in close agreement, with a mean absolute error of 2.7 %.

For further comparison, E_{atm} was also calculated using a non-spectral dependent model based on an effective broadband atmospheric emissivity. For this purpose, a calibrated version of the Brunt correlation was adopted [**?**]. As shown in Fig. S3a, the results obtained with this model are also in close agreement with the other signals.

The effective sky temperature can be expressed as:

$$T_{\text{sky}} = \bar{\varepsilon}_{\text{atm}}^{1/4} T_{\text{amb}} \tag{S5}$$

where $\bar{\varepsilon}_{atm}$ is the effective atmospheric emissivity. When $\bar{\varepsilon}_{\text{atm}}$ is evaluated over the entire infrared spectrum, the resulting temperature corresponds to the broadband effective sky temperature. Conversely, when it is evaluated only over the atmospheric window (AW), it represents the apparent sky temperature within the AW. Since the Earth's atmosphere is highly transparent within the AW but significantly more emissive outside this range, the apparent sky temperature in the AW is expected to be substantially lower than the effective broadband sky temperature.

Fig. S3b compares the temporal evolution of $\bar{\varepsilon}_{\text{atm}}$ evaluated over the entire infrared spectrum (using the calibrated Brunt and Das models) and over the AW only (using the Das model for 8–14 µm range). Fig. S3c compares the broadband sky temperature estimated using the calibrated Brunt and Das models with the AW sky temperature predicted by the Das model. The experimental measurements from the infrared sensor, which operates over the 8–14 µm spectral range wavelength range, are also reported. The AW sky temperature predicted by the Das model agrees well with the infrared measurements, except during the early hours of 6 September 2025, when the sky was not completely clear. This comparison validates the apparent sky temperature measurements obtained with the RAFT setup.

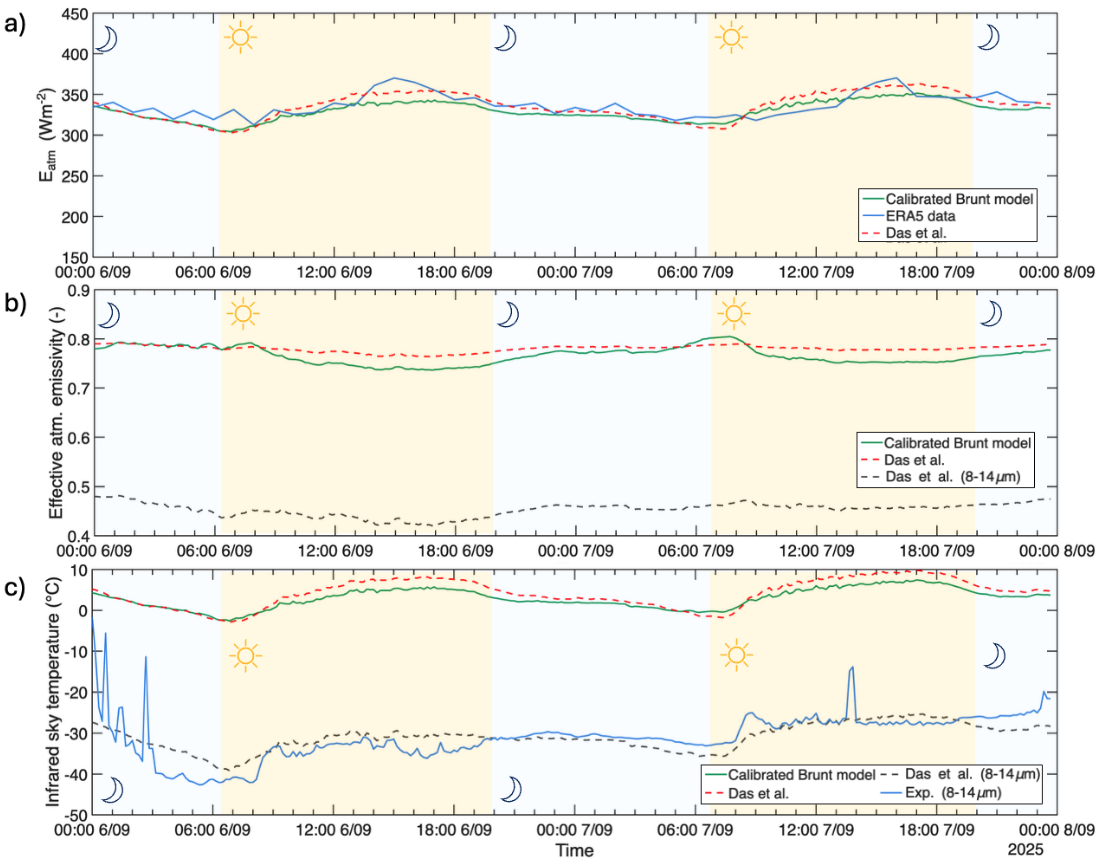

Figure S3: a) Modeled downwelling longwave atmospheric irradiance vs. data from ERA5 reanalysis database. b) Modeled effective atmospheric emissivity: broadband vs AW. c) Modeled sky temperature (broadband and AW) vs. experimental sky temperature measured by the infrared thermometer (operating in 8–14 µm range). All data refer to 6–7 September 2025, Turin.

S3. Error metric

This study employs the Mean Absolute Error (MAE) as the error metric to evaluate the agreement between experimental measurements and model predictions. The MAE is defined as:

$$\mathrm{MAE} = \frac{1}{n}\sum_{i=1}^{n} |y_i - \hat{y}_i| \,, \tag{S6}$$

where y_i represents the experimental value, $\hat{y}_i$ the corresponding model prediction, and n the total number of data points.

The metric is also employed to compare experimental data streams, specifically to assess whether the convective heat exchanger maintains the sample temperature equal to the ambient temperature.

S4. Supplemental Tables

Table S1: List of sensors used in this study

Instrument	Type	Parameter	Uncertainty
Heat-flux sensor	Hukseflux HFP01	Heat flux	±3 %
RTD	RS PRO Pt100	Thermal reservoir temperature	±0.01 °C
Digital multimeter	Keithley 2700	Voltage	±3.5 μV
Weather station	MAXIMET GMX501	Air temperature Relative humidity Wind speed Solar irradiance	±0.3 °C ±2 % ±3 % rms 1.8 %
Infrared thermometer (8–13 μm)	Optris CS LT	Apparent sky temperature	±1.5 °C

Table S2: Comparison of setup types for net heat flux measurements

Setup type	*Cooling* flux measurement	*Heating* flux measurement	Measurement stability near ambient temperature	User friendliness	Thermal guarding	Sample size dependence	Ref.
Resistive heater	Indirect	Not possible	Low	Medium	Not present by default	High/Medium	[5–8]
Heater-integrated heat flux meter	Direct	Not possible	Low	Medium	Embedded	Low	[9]
Flowing fluid	Indirect	Not possible	Good	Low	Not present by default	High	[10–13]
Peltier plate	Indirect	Indirect	Low	Medium	Not present by default	High/Medium	[14]
RAFT	Direct	Direct	Good	High	Embedded	Low	This work

References

[1] AK Das and M Iqbal. A simplified technique to compute spectral atmospheric radiation. *Solar Energy*, 39(2):143–155, 1987.

[2] AJ Prata. A new long-wave formula for estimating downward clear-sky radiation at the surface. *Quarterly Journal of the Royal Meteorological Society*, 122(533):1127–1151, 1996.

[3] John Monteith and Mike Unsworth. *Principles of environmental physics: plants, animals, and the atmosphere*. Academic press, 2013.

[4] H. Hersbach, B. Bell, P. Berrisford, G. Biavati, A. Horányi, J. Muñoz Sabater, J. Nicolas, C. Peubey, R. Radu, I. Rozum, et al. ERA5 hourly data on pressure levels from 1940 to present, Copernicus Climate Change Service (C3S) Climate Data Store (CDS). 2023d. Retrieved on December 1, 2025.

[5] Aaswath P Raman, Marc Abou Anoma, Linxiao Zhu, Eden Rephaeli, and Shanhui Fan. Passive radiative cooling below ambient air temperature under direct sunlight. *Nature*, 515(7528):540–544, 2014.

[6] Jérémy Werlé, Roberto Concas, Ernesto Pini, Diederik S Wiersma, Lorenzo Pattelli, and Giuseppe Emanuele Lio. Open-hardware platform for synchronous performance testing of multiple passive radiative cooling materials. *Cell Reports Physical Science*, 6(7), 2025.

[7] Yao Zhai, Yaoguang Ma, Sabrina N David, Dongliang Zhao, Runnan Lou, Gang Tan, Ronggui Yang, and Xiaobo Yin. Scalable-manufactured randomized glass-polymer hybrid metamaterial for daytime radiative cooling. *Science*, 355(6329):1062–1066, 2017.

[8] Jyotirmoy Mandal, Yanke Fu, Adam C Overvig, Mingxin Jia, Kerui Sun, Norman N Shi, Hua Zhou, Xianghui Xiao, Nanfang Yu, and Yuan Yang. Hierarchically porous polymer coatings for highly efficient passive daytime radiative cooling. *Science*, 362(6412):315–319, 2018.

[9] Minwoo Choi, Junyong Seo, Siwon Yoon, Youngsuk Nam, Jungchul Lee, and Bong Jae Lee. All-day radiative cooling using a grating-patterned PDMS film emitter. *Applied Thermal Engineering*, 214:118771, 2022.

[10] Eli A Goldstein, Aaswath P Raman, and Shanhui Fan. Sub-ambient non-evaporative fluid cooling with the sky. *Nature Energy*, 2(9):1–7, 2017.

[11] Dongliang Zhao, Ablimit Aili, Yao Zhai, Jiatao Lu, Dillon Kidd, Gang Tan, Xiaobo Yin, and Ronggui Yang. Subambient cooling of water: toward real-world applications of daytime radiative cooling. *Joule*, 3(1):111–123, 2019.

[12] Ablimit Aili, Dongliang Zhao, Jiatao Lu, Yao Zhai, Xiaobo Yin, Gang Tan, and Ronggui Yang. A kW-scale, 24-hour continuously operational, radiative sky cooling system: Experimental demonstration and predictive modeling. *Energy Conversion and Management*, 186:586–596, 2019.

[13] G Lopardo, F Bertiglia, G Braccialarghe, M Florio, F Girard, D Giraudi, F Santoro, and L Pattelli. Metrological setup for accurate determination of passive radiative cooling power. *Applied Thermal Engineering*, page 130363, 2026.

[14] Xiuqiang Li, Bowen Sun, Chenxi Sui, Ankita Nandi, Haoming Fang, Yucan Peng, Gang Tan, and Po-Chun Hsu. Integration of daytime radiative cooling and solar heating for year-round energy saving in buildings. *Nature communications*, 11(1):6101, 2020.